

Search for x-ray induced decay of the 31-yr isomer of ^{178}Hf using synchrotron radiation

I. Ahmad,¹ J. C. Banar,² J. A. Becker,³ T. A. Bredeweg,² J. R. Cooper,³ D. S. Gemmell,¹ A. Kraemer,³ A. Mashayekhi,⁴ D. P. McNabb,³ G. G. Miller,² E. F. Moore,¹ P. Palmer,² L. N. Pangault,² R. S. Rundberg,² J. P. Schiffer,¹ S. D. Shastri,⁴ T.-F. Wang,³ and J. B. Wilhelmy²

¹Physics Division, Argonne National Laboratory, Argonne, Illinois 60439, USA

²Los Alamos National Laboratory, Los Alamos, New Mexico 87545, USA

³Lawrence Livermore National Laboratory, Livermore, California 94550, USA

⁴Advanced Photon Source, Argonne National Laboratory, Argonne, Illinois 60439, USA

(Received 9 September 2004; published 24 February 2005)

Isomeric ^{178}Hf ($t_{1/2} = 31$ yr, $E_x = 2.446$ MeV, $J^\pi = 16^+$) was bombarded by a white beam of x rays from the Advanced Photon Source at Argonne National Laboratory. A search was made for x-ray induced decay of the isomer by detecting prompt and delayed γ rays associated with the decay. No induced decay was observed. Upper limits for such a process for x-ray energies between 7 and 100 keV were set. The limits between 7 and 30 keV are below $\approx 3 \times 10^{-27}$ cm² keV for induced decay that bypasses the 4-s isomer and $\approx 5 \times 10^{-27}$ cm² keV for induced decay that is delayed through this isomer, which are orders of magnitude below values at which induced decay was reported previously. These limits are consistent with what is known about the properties of atomic nuclei.

DOI: 10.1103/PhysRevC.71.024311

PACS number(s): 23.20.-g, 23.90.+w, 25.20.Dc, 27.70.+q

I. INTRODUCTION

Since the enormous success of nuclear fission reactors over 60 years ago, other ways to control the release of energy stored in nuclear binding have been of continuing interest. Thus, controlled fusion of isotopes of hydrogen has been the subject of major undertakings since the 1950s. Other approaches have looked promising at various times and have stirred considerable interest, for instance when the implications of reports for achieving fusion at room temperature were considered, but these reports were quickly disproven.

Nuclear isomers offer an intriguing area for investigation, partly because of their potential as an energy source and partly because of the continuing hope that if the release of energy could be controlled, γ -ray lasers may perhaps be feasible. The report that the irradiation of the 31-yr isomer of ^{178}Hf with x rays from a dental x-ray machine enhanced the decay rate [1] aroused considerable interest. While this would represent less energy per nucleus than would be available in fission, its implications, for instance, in aircraft propulsion [2,3], have been discussed. This isomer has the highest stored energy for a long (more than a year) half-life. More recently, considerable controversy has arisen over the speculation [3] that a new global arms race could be triggered by the development of new types of nuclear weapons and other military and civilian applications based on triggered isomer decays.

The report of triggered isomer decay was quickly followed by criticisms of the rates, partly because of the limited statistics and also because such a phenomenon would violate well-established rules about nuclear electromagnetic transitions. In fact, the reported transition rates would have to be about a million times stronger than known transitions in this energy range and come close to exceeding sum rules that are based only on the charge, mass, and size of the nucleus [4]. However, subsequent measurements by the original group were positive,

though the statistical significance did not greatly improve [5,6]. More recently, researchers [7,8] suggested that this effect may be due to an indirect electronic process (NEET) where the electronic excitation is transferred to the nucleus since the energies in the more recent results were near the L-absorption edge. However, a recent calculation [9] of such a process for Hf indicates that this mechanism is unlikely.

The present report describes experiments searching for such triggering under greatly improved conditions with a white x-ray beam that covers the whole relevant wavelength region and has an intensity about five orders of magnitude greater than that used in the original report [1]. Our first measurement [10] showed no sign of triggered decay with cross-section limits again some five orders of magnitude lower than those that had been originally reported.

A subsequent measurement was made by the original group [7], also at a light source, but with a monoenergetic x-ray beam whose energy could be varied through a monochromator. Enhanced decays were again reported, but induced with 9–13-keV x rays, considerably lower in energy than reported originally. We then repeated the measurement with the white x-ray beam, but this time with a substantially thinner target in which there could be no question of absorption effects at the low x-ray energies. We again found no enhancement [11–13].

The electromagnetically induced decay of an isomer of ^{180}Ta was found by a different group [14] using bremsstrahlung photons with a 1-MeV or higher endpoint (instead of 20–60-keV photons). The rate observed in this Ta measurement is consistent with expectations and much lower than the results reported in [1].

The purpose of the present publication is to give the details of the two measurements [10,11] carried out at the Advanced Photon Source (APS) with white x-ray beams, details that could not fit into the abbreviated Letter and Rapid Communication reports that initially reported our findings.

TABLE I. Strongest enhanced $^{178}\text{Hf}^{m2}$ transitions in publications of Collins *et al.*

X-ray source	Lines feeding 4-s isomer (Enhancement)	G.S. band (Enhancement)	New lines	Integrated cross section (Energy range)
Dental x ray [1]	495 keV ($6.3 \pm 2.2\%$)	426 keV ($2.0 \pm 1.3\%$)	—	$1 \times 10^{-21} \text{ cm}^2 \text{ keV}$ (if $\sim 40 \text{ keV}$)
Dental x ray [5]	217 keV ($1.6 \pm 0.3\%$ combined)	213 keV	—	$>2.2 \times 10^{-22} \text{ cm}^2 \text{ keV}$ (if $<20 \text{ keV}$)
Dental x ray [15]	—	213 keV (lines in coincidence)	129 keV	Not given
SPring-8 [7,8]	217 keV ($3.0 \pm 0.7\%$ combined)	213 keV	—	$(1.8 \pm 0.4) \times 10^{-22} \text{ cm}^2 \times 0.13 \text{ keV}$ (for 11.3 keV region) $(2.0 \pm 0.5) \times 10^{-22} \text{ cm}^2 \times 0.12 \text{ keV}$ (for 11.7 keV region) $(3.2 \pm 0.7) \times 10^{-22} \text{ cm}^2 \times 0.07 \text{ keV}$ (for 9.56 keV region)

The journal publications of positive results for triggering are summarized in Table I, with the cross sections being those quoted; the widths of the energy intervals for the regions of enhancement were obtained from the published figures.

II. PROPERTIES OF ^{178}Hf

The 31-yr isomer of the nucleus ^{178}Hf , labeled $^{178}\text{Hf}^{m2}$, is a K isomer with $J^\pi, K = 16^+, 16$ at an excitation of 2.446 MeV. Its normal decay has been studied extensively [16]. Figure 1 shows the relevant energy levels and band structure in ^{178}Hf [17]. The 16^+ isomeric state decays primarily through an $E3$ transition to the 13^- member of the $K = 8$ band whose $J^\pi = 8^-$ bandhead is itself an isomer decaying with a 4-s half-life primarily to the 8^+ member of the ground-state band (GSB), followed by a cascade to the ground state. One of the first hypotheses offered by Collins *et al.* for their observation of accelerated decay postulates a state (or states) of mixed K values, excited from the 16^+ isomeric state by resonant absorption of x-ray photons with energies in the range 20–60 keV. Such an intermediate state then may decay to a lower-lying level in the $K = 8$ band and then to the 8^- bandhead, whose deexcitation with a 4-s half-life cascades in a well-known way, down through the GSB.

In addition to the levels populated in the decay of $^{178}\text{Hf}^{m2}$, Fig. 1 shows levels which have been observed to directly populate the $K^\pi = 16^+$ isomer. The $K^\pi = 14^-, 68\text{-}\mu\text{s}$ isomer has been observed to decay to the $K^\pi = 16^+$ isomer with a partial half-life of 110 μs via a 126-keV transition ($\approx 94\%$ electron converted) [17]*. Rotational band members built on the $K^\pi = 16^+$ bandhead have also been observed [18–21]. The $17^+ \rightarrow 16^+$ transition had been measured in heavy-ion multiple Coulomb excitation to have a reduced $E2$ transition probability of $B(E2) = 5.9(8)e \text{ b}$ [19]. In addition, the 15^- and 16^- rotational band members built on the $K^\pi = 14^-$

bandhead were also observed [20]. These states are the only known candidate states for x-ray resonant absorption, i.e., $^{178}\text{Hf}^{m2}(\gamma, \gamma')$ resonance scattering. None of these states is within 60 keV of the $^{178}\text{Hf}^{m2}$ isomer, and only the $K^\pi = 14^-$ band has a decay path that bypasses the $K^\pi = 16^+$ isomer. It seems unlikely that there could be a significant number of unknown levels that would be accessible by $E1$ resonant absorption.

As mentioned above, theoretical estimates of the cross section for indirect electronic deexcitation of this isomer via the NEET mechanism [9] produced values that are, at best, in the realm of 10^{-32} cm^2 , some 10 orders of magnitude lower than the effects reported by Collins *et al.*

III. THE EXPERIMENT

A. Overview

White beams were obtained from the Advanced Photon Source (APS) by employing a tapered gap setting in the 2.5 m long undulator insertion device (undulator A [22]) at the XOR 1-ID beamline. The maximum taper (5 mm) of the device was used. This means, for example, that for an average gap width of 15 mm, the gap was 12.5 mm at one end of the device and 17.5 mm at the other. A tapered gap causes the sharply structured spectrum of the beam from the insertion device to be “smeared out” in energy. However, some structure still remains and, to ensure that the entire x-ray spectrum range in question was covered adequately, leaving no “local minima,” two gap settings, with average settings of 15 and 20 mm, were used. Some data were also collected with an average gap of 13.5 mm. (See Sec. III E for a more detailed discussion of the photon beam.)

Initially, as summarized in Table I, the reported positive observations of the triggering effect indicated that the triggering took place in the energy range 20–60 keV, so our first attempts at verification were designed to be optimally sensitive in this energy range. These measurements were valid down to about 8 keV, but sensitivity decreased below about 15 keV because of absorption effects of the incident photon beam in various beamline windows and in the target itself. Subsequent publications [7,8] reported enhancement in the

*Derived from the sum of the observed γ -ray intensities of the 216.7- and 454.0-keV lines feeding the $J^\pi = 8^-$, 4-s isomer. A correction for conversion electrons was applied using the values suggested in [17].

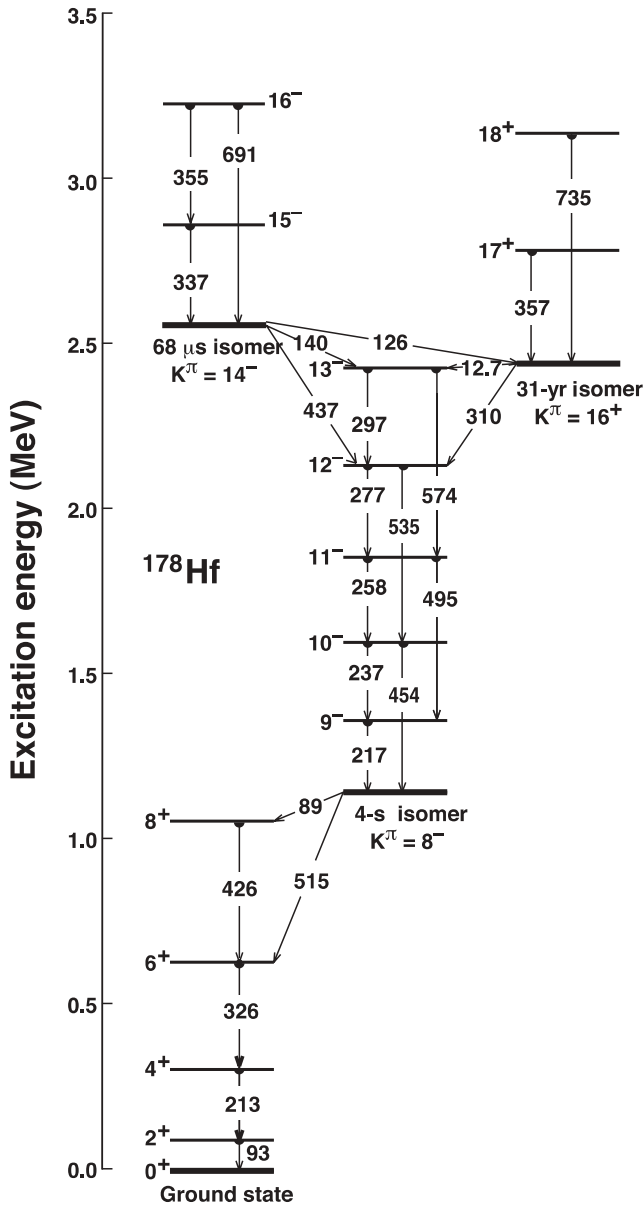


FIG. 1. Energy level diagram showing the decay path of the 31-yr ^{178}Hf isomer. Some higher transitions that are known to feed the isomer are also shown. Transition energies are shown in keV.

region below x-ray energies of 15 keV (see Table I). Our second set of measurements used a new target design such that absorption corrections were minimized and the overall sensitivity was optimized for beam energies in the range 7–20 keV. In the remainder of this publication, we will refer to the first experiment [10] as the thick-target measurement, and the second one [11] as the thin-target measurement. Detailed descriptions of both target configurations are provided in Sec. III D.

Any triggered decay of the 31-yr isomer of ^{178}Hf would most likely proceed through the known $K^\pi = 8^-$ isomer whose bandhead has a half-life of 4 s. Indeed, the largest observed enhancement (6.3%) proposed as being due to triggering was reported by Collins *et al.* [1] for the 11^- to 9^- ,

495-keV transition in this band. Our measurement strategy was therefore designed to optimize the sensitivity for obtaining information on a possible enhancement of this decay mode. The measurements were repeated on a cyclic basis, each cycle composed of three time periods (one for irradiation, and two for counting with the beam off). To maximize the overall statistical significance, we calculated that the optimal arrangement was to use three periods, each of duration equal to 2.9 times the 4-s half-life of the $K^\pi = 8^-$ isomer bandhead. Therefore, when combined with the time associated with the shutter movements, the measurements were cycled in three 10.6-s intervals: the x-ray beam on the target for 10.6 s, and then two successive periods of counting for 10.6 s each. Briefly stated, the idea was that the first time period (T_1 , beam on) would allow the buildup of a beam-induced population of the 4-s state. This population would be detected as it decayed away during the second period (T_2 , beam off). The third period (T_3 , also beam off) served mainly to establish the background counting rate.

While this was the primary mode of measurement, the experiment was arranged to be simultaneously sensitive to any prompt beam-induced decays, i.e., decays that may have bypassed the 4-s isomeric state. This was achieved by measuring the counting rate during the first period (beam on). The accuracy obtained for promptly induced decays was somewhat lower than for those that were delayed because of the higher background rate with the beam on than with the beam off.

B. Experimental arrangement

1. Thick-target experimental arrangement

The first set of our measurements involved thick targets, consisting of a mixture of HfO_2 and Al powder, described in more detail below. The experiment involved irradiating several targets containing different amounts of Hf at two undulator-gap settings. Data were accumulated over a period of about 10 h for each target-undulator combination. The target thickness and the undulator settings were varied to enhance different energy regions with the x-ray beam. Measurements with the thinnest of the targets and largest undulator-gap settings had the greatest sensitivity for decay induced by the low-energy component of the x-ray beam.

A schematic diagram of the experimental setup is shown in Fig. 2. The target assembly was tilted at 15° from the plane perpendicular to the beam direction. Two planar germanium detectors were mounted at 90° to the beam and surrounded by lead bricks to minimize counts from the scattered beam. The detector characteristics and shielding configurations are described in Sec. III C. The beam was cycled on and off the target by moving a W block so that the beam passed through the hole or was blocked; this motion took about 1.5 s. In each cycle, the beam irradiated the target for 10.6 s (T_1) and then it was off for ≈ 24 s with two periods of out-of-beam counting and allowing time for the motion of the W block.

While the beam was on, the Pb shutters were in front of the detectors to protect them from being overwhelmed by scattered beam, though one of the shutters had a small hole (not shown)

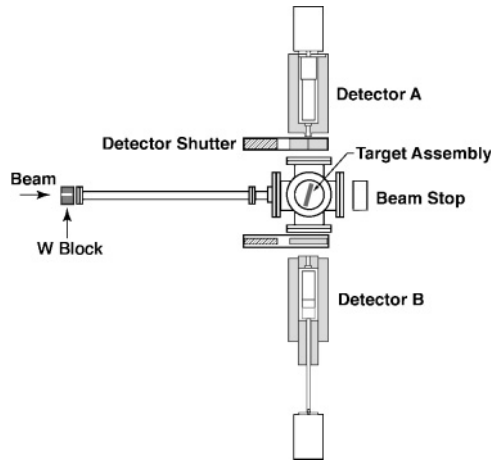


FIG. 2. Schematic diagram of the experimental setup for the thick-target run. The lead shielding is shown in gray, and the hatched area indicates the position of the movable shutters when the beam was off.

to monitor the x-ray yield at a tolerable count-rate level. When the beam was off target, the detector shutters were moved aside using compressed air. The motion of the detector shutters was synchronized with the movement of the W block and also required about 1.5 s. Data recorded during the movement of the shutters were excluded in the off-line analysis for 1.6 s.

2. Thin-target experimental arrangement

In the second, thin-target experiment with a thin layer of HfO_2 sandwiched between Be disks (as described in Sec. III D), the setup was very similar to that described above and is shown in Fig. 3. The measurement was performed using one $^{178}\text{Hf}^{m2}$ target optimized for sensitivity to x-ray energies between 7 and 20 keV, as described in the following section. The white beam from a tapered undulator was collimated to $1.4 \times 2 \text{ mm}^2$ and entered the target chamber through a 0.25-mm-thick Be window. The target assembly was oriented at 45° with respect to the beam, and the beam illuminated a $2 \times 2 \text{ mm}^2$ area of the target. The beam was cycled on and off the target by moving the W block with the same time intervals as those in the thick-target experiment.

Two photon detectors (one planar germanium and one Si(Li) x-ray detector) were placed at 90° to the beam and surrounded by Pb bricks. Each detector viewed the target through collimators and absorbing shields (see Sec. III C). In contrast to the thick-target measurement, moving shutters were not used in front of the detectors since the scattering of the beam by the thinner target was greatly reduced.

C. Detector configuration

1. Thick-target detector configuration

X rays and γ rays emitted from the target were measured using two planar Ge detectors, A and B, mounted on opposite sides of the target in the horizontal plane and at 90° to the

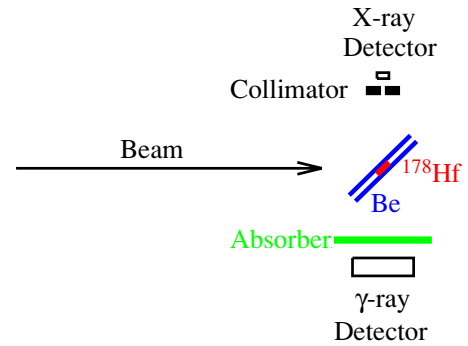


FIG. 3. (Color online) Schematic diagram of the experimental setup for the thin-target run. The shielding around the two detectors is not shown.

incident beam (see Fig. 2). The Ge crystals were both 51 mm in diameter and their thicknesses were 17 mm (A) and 15 mm (B). The distances from their front faces to the target were 36 and 39 cm, respectively.

To shield the detectors as well as possible from the scattered beam, each detector was surrounded by a 5-cm-thick lead housing that had an opening that gave the detector a collimated view of the radioactive target. The collimators ranged from 2 to 4 cm in diameter, depending on beam conditions and the activity of the target. Pb shields 2.54 cm (1 in.) thick (A) and 1.27 cm (1/2 in.) thick (B) were moved in front of the collimated openings in the lead housing during the beam-on part of the cycle. In the case of detector A, the shield contained a 2.4-mm-diameter collimating hole to permit monitoring of the beam-induced Hf x rays, and observing the x rays with this detector was also used in aligning the target with the x-ray beam. Pb, Ta, Gd, Sn, Mo, Cu, and Al absorbers were introduced as needed to reduce total counting rates to a few thousand per second in the beam-on configuration. A summary of the detector configurations and counting rates is presented in Table II.

An example of efficiency curves for detector A in both in-beam and out-of-beam counting configurations, determined from the known activity of one of the radioactive targets (R-2; see Sec. III D) with no beam present, is shown in Fig. 4. The decrease in detector efficiency below 200 keV is due to attenuation in the target assembly and the absorbers. The open- and closed-shield detector efficiencies were also simulated using the Monte Carlo N -particle (MCNP) transport code [23], taking into account all the absorber materials, the geometry of the setup, and the detector configuration as specified by the vendor. The agreement between the simulated and measured efficiency is better than 10% in both cases, as seen in Fig. 4.

2. Thin-target detector configuration

The thin-target detector configuration was similar to that used in the thick-target experiment with two main differences: (i) a single Ge detector (51 mm diameter \times 15 mm thick) and one Si(Li) detector (10 mm diameter \times 5 mm thick) were used and (ii) no moving shutters were required in front of the detectors at any time during the cycle (see Fig. 3). The

TABLE II. Summary of Ge detector configurations and typical total counting rates for each target and gap setting. Note that the same-sized collimators were used for Ge detectors A and B in the thick-target experiment (R-1, R-2, and R-3), and only one Ge detector was used in the thin-target experiment (RH-3).

Target	Average undulator gap (mm)	Detector collimator (cm)	Beam-on rate (kHz)		Beam-off rate (kHz)	
			Det. A	Det. B	Det. A	Det. B
R-1	20.0	4	15	2.0	1.3	1.3
R-1	15.0	4	26	26	0.9	1.8
R-2	20.0	3	9.3	1.7	1.4	3.3
R-3	20.0	2	4.6	1.0	2.4	2.8
R-3	15.0	2	44	11	2.3	3.0
R-3	13.5	2	11	2.8	2.4	2.9
RH-3	20.0	3	5.8	—	<0.1	—
RH-3	15.0	3	18	—	<0.1	—

planar Ge detector, located at 90° and at a distance of 22.9 cm, viewed the target through a 6.3-mm-thick Plexiglas window. To keep the count rate in the Ge detector to manageable levels during the irradiation period, a 3.0 cm diameter collimator was used in conjunction with composite absorbers consisting of various thicknesses of Pb, Ta, Cd, Cu, and Al to reduce the intensity of the scattered x-ray beam as given in Table III, where the two entries for the 15-mm gap refer to the two absorber configurations that were used to emphasize different parts of the spectrum.

The photopeak efficiency for the Ge detector configuration used for the 20-mm-gap beam setting was measured with a calibrated source and is presented in Fig. 5. Also shown is the result of an MCNP simulation for this arrangement, with the absorbers listed in Table III included. The good agreement between the measured and simulated efficiency values allows extrapolation down to energies around 125 keV, where the absorber thickness and low source strength prevented the direct measurement of the detection efficiency for the 125.8-keV line from ^{172}Hf . The calculated detection efficiency is used to set

limits on the reported [15] stimulated emission of a new, and previously unknown, 129-keV line during irradiation. This line is not seen in a detailed counting of $^{178}\text{Hf}^{m2}$ [24].

On the opposite side of the chamber, the Si(Li) detector viewed the target through a 0.5-mm-thick Be window from a distance of 47.6 cm to the beam axis. A $0.05 \times 0.05 \text{ mm}^2$ collimator was placed in front of the Si(Li) detector to reduce the in-beam counting rate to a manageable level. The purpose of the Si(Li) detector was to monitor the fluorescent x rays from the target as a measure of the beam luminosity. This monitor was also used in aligning the target with the beam by moving the target through the beam horizontally and vertically, while monitoring the characteristic x-ray yield.

D. Targets

The Hf used in the targets was extracted from Ta beam stops at the LAMPF accelerator at Los Alamos National Laboratory. The Hf was chemically extracted from the Ta beam-stop material, purified, precipitated, and converted into HfO_2 for use in the present experiment. In addition to the

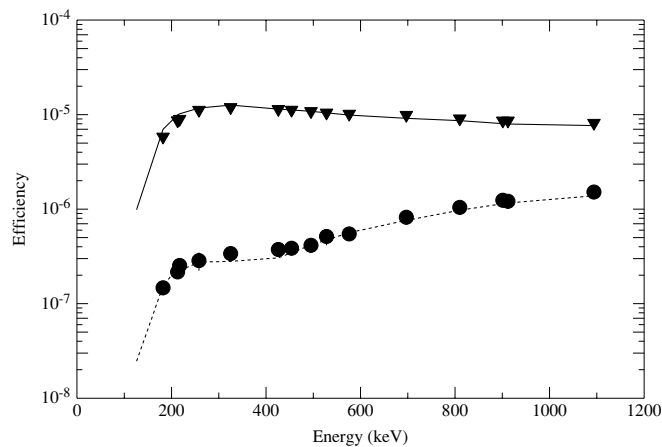


FIG. 4. Measured absolute photopeak efficiency for the thick-target detector A in the beam-on, shutter closed (dots) and beam-off, shutter open (triangles) configurations, with the error bars smaller than the size of the points. The solid and dashed lines show the efficiencies calculated with the MCNP code.

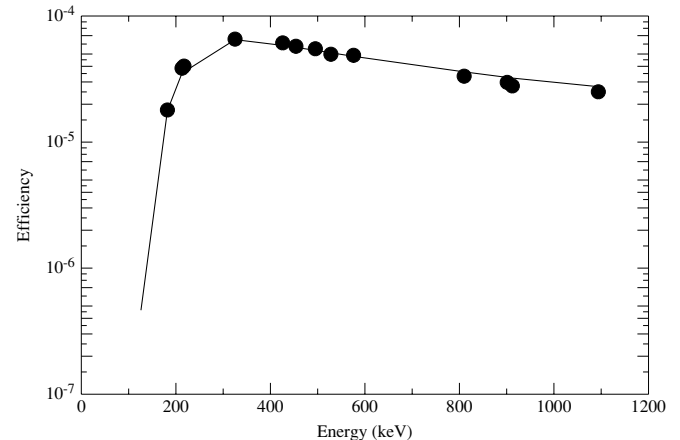


FIG. 5. Absolute photopeak efficiency of the Ge detector used in the thin-target experiment, configured for the 20 mm gap beam setting with the absorber configuration shown in Table III. Measured values (points), with error bars smaller than the size of the points, and the MCNP simulations (line) are shown.

TABLE III. Summary of absorber sheets placed in front of the Ge detector for each gap setting used in the thin-target experiment. The absorbers were ordered such that the Pb sheet was facing the target in each case.

Average gap (mm)	Pb (mm)	Ta (mm)	Cd (mm)	Cu (mm)	Al (mm)
20	1.78	0.101	1.09	1.63	1.59
15(a)	5.6	0.127	1.09	1.63	1.59
15(b)	3.2	0.127	—	—	—

31-yr $^{178}\text{Hf}^{m2}$ isomer, the target contained some stable Hf from impurities in the beam stop. In addition, the spallation reaction also produced other Hf isotopes, including ^{172}Hf ($t_{1/2} = 1.89$ yr), that proved useful in monitoring the target during the experiment.

The target material contained 0.38 mg of $^{178}\text{Hf}^{m2}$ per gram of stable hafnium. Two types of $^{178}\text{Hf}^{m2}$ targets were used. The thick target, shown in Fig. 6, was designed to maximize the probability of observing accelerated decay by interaction with high-energy x rays. These targets consisted of hafnium oxide powder mixed with aluminum powder to improve heat conductivity. The mixtures were tamped into a 2-mm-diameter hole with a depth of 1.6 mm. The remaining volume was filled with aluminum powder and covered with a 0.15-mm aluminum foil. The targets using this design were designated as R-1, R-2, and R-3. The total thicknesses, including the filler and cover foil along with the hafnium oxide amounts, are listed in Table IV.

The thin target type was designed to improve sensitivity to accelerated decay by interaction with low-energy x rays. The thin-target assembly is shown in Fig. 7. These targets consisted of thin spots of hydrous hafnium oxide, 2 mm in diameter, electrodeposited onto two 0.5-mm-thick Be disks. Beryllium was chosen to minimize the absorption of low-energy x rays. The Be disks were flashed with a layer of titanium ~ 1000 Å thick to improve electrodeposition. The two disks were mounted clamped together, with the deposits facing each other. The target of this type designated RH-3 was used in these measurements. The target thicknesses are listed in Table IV with the Hf activities measured some weeks after the measurements, though the activities were also assayed before the measurement to ensure that none was lost.

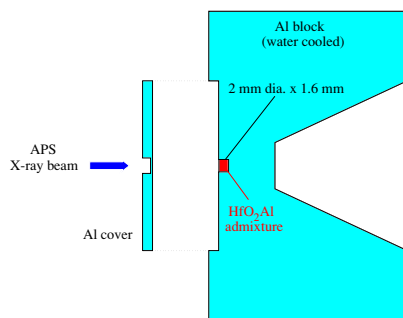


FIG. 6. (Color online) Schematic diagram of the thick-target assembly.

1. Target heating

The power in the x-ray beam incident on the targets was limited to a maximum of ~ 210 W. In order to provide sufficient target cooling in the thick-target measurement, a massive water-cooled aluminum block was used. To estimate the temperature of the hafnium oxide in the target assembly, the target shape was approximated as being either a cylinder or sphere. Analytic solutions to the heat-conduction equation exist for both of these geometries.

If we assume, in a first approximation, that the synchrotron radiation is uniformly absorbed in a cylinder of radius a and that the water cooling maintains a constant temperature in the cooling block at radius b , then the heat flowing across a cylindrical surface of length h from the inner cylinder is

$$Q = \frac{-2\pi ahK(T_a - T_b)}{\ln(b/a)}, \quad (3.1)$$

where K is the thermal conductivity per unit area and T_a and T_b are the temperatures at these radii.

The actual target assembly is more massive and occupies more volume than a cylindrical geometry. It could alternatively be approximated as a sphere where the energy is deposited in an inner sphere with radius a and cooled to a lower temperature

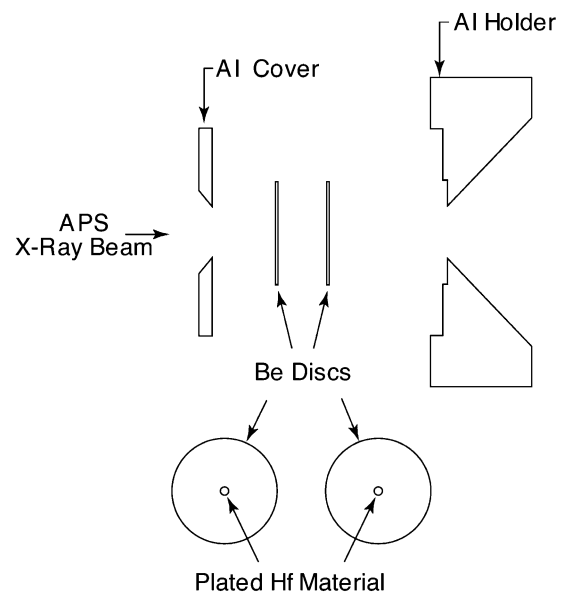


FIG. 7. Schematic diagram of the thin-target assembly.

TABLE IV. Target composition.

Target	Target thickness (mg/cm ²)	Content (%)			Activity (Bq)	
		Hf	O	Al	¹⁷⁸ Hf ^{m2}	¹⁷² Hf
R-1	360	6	1	93	5.2×10^5	1.12×10^6
R-2	400	19	3	78	2.1×10^6	4.6×10^6
R-3	450	34	6	60	4.5×10^6	9.7×10^6
RH-3	0.55	85	15	—	1.3×10^4	1.55×10^4

at a radius b . In this case,

$$Q = \frac{-4\pi abK(T_b - T_a)}{(b - a)}. \quad (3.2)$$

The x-ray spectrum was calculated and is discussed below. The photon absorption coefficients were calculated using the National Institute of Standards and Technology (NIST) code XCOM [25]. Scattering out of the target was not considered. The target material was approximated as a uniform cylinder of thickness and composition listed in Table IV. The thermal conductivity of the aluminum block is 2.37 W/cm K. The conductivity of beryllium is 2 W/cm K. The part of the aluminum block containing the hafnium target was thinned to minimize photon scatter about a radius of 0.33 cm from the center of the target for the thick targets. This distance was used as the outer boundary for heat conduction. The depth of powder targets was 0.16 cm. The targets deposited on beryllium were mounted on a water-cooled aluminum block with a 1.25-cm-diameter hole behind it. The boundary was thus chosen to be 0.64 cm for the thin targets. The results of the heat conduction calculations are shown in Table V for the power from the 15-mm-gap setting. The power with the 20-mm-gap settings was lower, and consequently the corresponding temperature rises are lower by almost a factor of 2.

The cooling-water temperature was 15 °C. Based on the results reported in Table V, the highest temperature would be 93 °C for the 15-mm-gap setting and some data were obtained at about 50 °C. With the 20 mm gap, some of the data were taken below 40 °C. For the thin-target measurement the estimated temperature rise was less than 30 °C.

2. Target stoichiometry and alignment

For the thick targets, the hafnium oxide and aluminum powder were weighed before mixing. Target activities were

TABLE V. Target temperature estimates.

Target	Dissipated power (W)	Temperature rise (°C)	
		Cylindrical appr.	Spherical appr.
R-1	79	40	36
R-2	130	64	60
R-3	159	78	74
RH-3	8.8	13	29

measured with a germanium detector in a calibrated geometry. The calibrated detector viewed the front face of the target assembly in order to minimize attenuation effects. The activity of each species, ¹⁷⁸Hf^{m2} and ¹⁷²Hf, was determined from a weighted average of γ -ray lines with energies above 180 keV. Branching ratios were taken from [17,26]. The mass measurements and known enrichment were consistent with the measured activity.

Each target was carefully aligned with the photon beam by maximizing the yield of beam-induced hafnium K -x-rays. These Hf K -x-rays were used as an in-beam monitor of the photon flux on the target material in all measurements and are compared to the calculated flux in Sec. III E.

E. Photon beam

During the thick-target measurement, the stored electron beam of the APS was maintained at a steady 100 mA through the use of a continuous “top-up” mode of operation. The undulator was operated with maximum taper (a total of 5 mm) in the gap and most of the irradiations were performed with average gap settings of 15 and 20 mm (Fig. 8); the sharp energy structure inherent in undulator radiation was largely smoothed out by the tapering. The use of different gap settings filled in the remaining variations of photon intensity with energy.

For the thick target, the horizontal and vertical slits were set at 1.5 mm. After passing through a 1.5-mm-thick carbon disk and a Be window, the beam entered the XOR 1-ID-B station, and while in air, it passed through a movable tungsten block with a 3-mm-diameter hole. The beam then passed through a 0.25-mm Be window (not explicitly shown in Fig. 2) into an evacuated beampipe and then through another 0.25-mm Be window into the He-filled target chamber. The total thickness of Be was 1.5 mm. In addition, the cover foil of the target material was 0.15 mm of Al. When the average undulator gap was 13.5 mm, an additional 6.35 mm of copper was inserted in the beamline and the slits were moved to 0.75 mm to reduce the beam intensity at the target (preliminary test measurements had established the safe limits for beam intensity, beyond which melting and rupture of parts of the target assembly became a possibility).

For the thin-target measurements, the horizontal slits were set at 1.05 mm and the vertical ones at 1.5 mm. For the 20-mm-gap setting, no carbon absorber was used; but for the 15-mm-gap, a 1.5-mm carbon disk was inserted. The total thickness

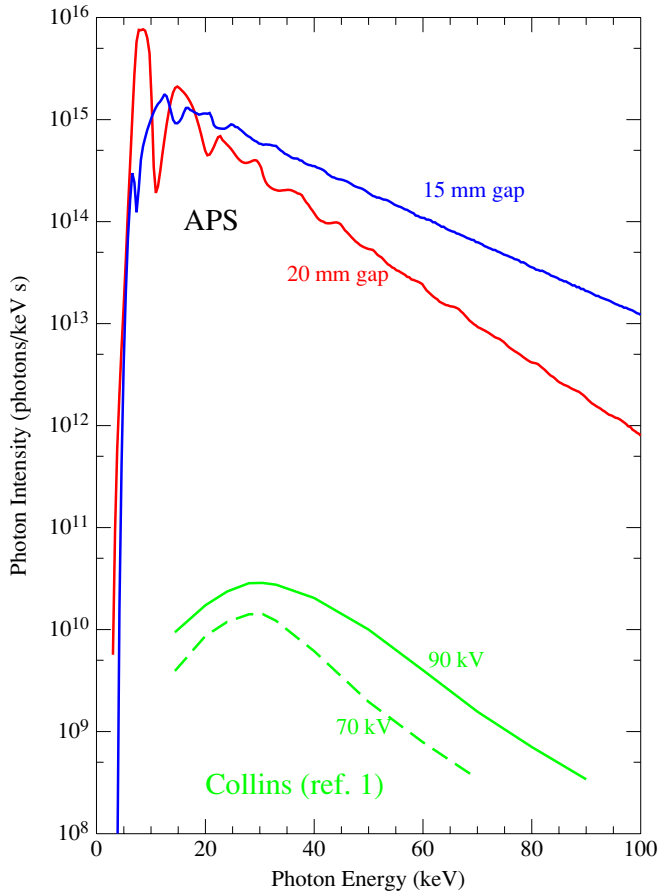


FIG. 8. (Color online) The calculated beam spectrum from the Advanced Photon Source incident on the Hf target material in the thin-target measurement, for two tapered settings of the undulator gap that were used and with a 100-mA circulating current. The photon intensities, given in Refs. [1,30] for the 70- and 90-kV setting of the dental x-ray machine on a 1-cm-diameter target, are also shown.

of Be, including the first target disk, was 2.2 mm, and the thickness of Ti was 0.14 μm .

The photon flux and spectral properties of the x-ray beam emerging from the undulator have been measured on several occasions (for example, in [27]) and have been found to agree well with the predictions of the so-called UR code, a well-tested computer program that calculates these quantities using Monte Carlo methods [28]. The beam spectra shown in Fig. 8 for average undulator gaps of 15 and 20 mm are those calculated to exist at the interface between the 0.15 mm Al entrance window of the target assembly and the HfO₂ and Al powder mixture. At this interface, the power in the beam was calculated to be 192 W (15-mm gap) and 81 W (20-mm gap).

To check that the beam luminosities achieved in the measurements agreed with calculated values, the yield of characteristic Hf *K* x rays was measured in one of the Ge detectors while the average gap in the undulator was set to 20 mm. Measurements were made with target R-1 (see Table II). The beam intensity incident on the target powder and its energy profile were as shown in [10] for the 20-mm gap. The target assembly was tilted slightly (15°) toward the detector and the total live time for the measurement was 2000 s.

The experimental arrangement was as described in Sec. III B. Absorbing layers of 6.35-mm (1/4-in.) Cu and 25.4-mm (1-in.) Al were inserted between the 2.4-mm collimating hole and the front face of the detector. This measurement showed that the rate of emission of Hf *K* x rays was 2.8×10^{12} per second for a stored electron current in the ring of 100 mA. For comparison, the calculated rate, taking into account factors such as absorption of the beam and of the emitted x rays in the target material and in the Al target assembly, was 3.1×10^{12} per second.

The major sources of error in these calculations lie in the cross sections used for *K*-vacancy production and for absorption. We have employed the tabulations of Chantler [29], which are believed to be accurate to about 1%. This leads to errors on the order of 10–20% in the absorption factors. The fact that the measured and the calculated *K*-x-ray yields agree to within about 10% is a good indication that the beam intensity, the target compositions, and the physical overlap of the beam with the target are well understood.

In the thin-target experiment, the APS ring was filled at roughly 12 h intervals to a maximum stored beam current of 100 mA. The current steadily declined to about 60 mA just prior to the next fill of the ring current. Tapered gap settings with average gaps of 15 and 20 mm and a taper of 5 mm were used, as described above. The transparency of the system to low-energy x rays was verified through a measurement made with a thin Cu target evaporated onto Be. Because the *K* x rays in Cu are low in energy (~ 8 –9 keV), their measured yields are sensitive to the low-energy component in the beam: the flux below 10 keV is responsible for 50% of the *K*-x-ray yield; the flux below 20 keV, for 86%. We found that the observed and calculated Cu *K*-x-ray yields are consistent to within a factor of 2, which is satisfactory agreement given the uncertainties arising from the very tight collimation of the Si(Li) detector (see Sec. III C).

As a check on the calculated energy profile that was produced with the tapered undulator, shown in Fig. 8, measurements were made after the data collection in the thin-target runs with a monochromator and ionization chamber. This was done by scanning a Si(311) monochromator in energy between 11 and 15 keV, and recording the transmitted intensity with a N₂ ionization chamber. The ionization chamber current was corrected for ion-chamber efficiency, for the monochromator bandwidth from perfect crystal diffraction theory, and for heat load and/or mounting-induced lattice strain. Figure 9 presents the calculated and measured energy distributions of the x-ray beam profile for the two tapered undulator settings. The level of agreement (20–30%) is satisfactory considering the approximations made regarding the magnetic fields in the tapered undulators and other uncertainties.

The principal systematic errors in the overall luminosity for the beam incident on hafnium include the precise shape of the photon spectrum, the magnitude of corrections for absorption along the beam path, and any small uncertainty in the exact overlap of the hafnium in the target with the beam. A precise analysis depends on the photon energy, but we estimate that the overall systematic uncertainty is 30% over the energy range between 7 and 100 keV for the thin target, and 45% for the range of 20–100 keV for the thick target.

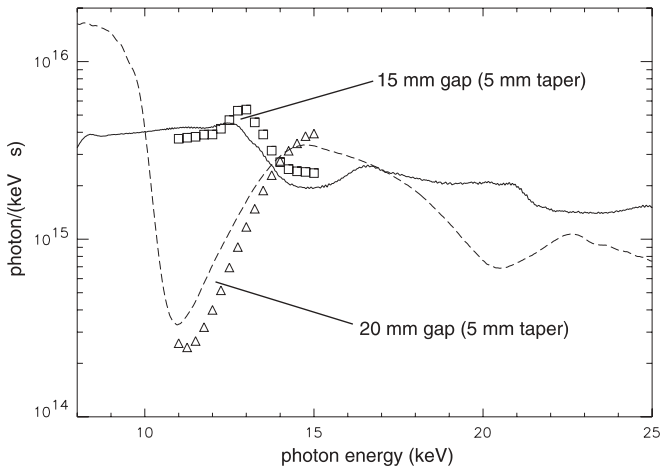


FIG. 9. Comparison of the calculated (line) and measured (symbols) x-ray energy profile from the two settings of the tapered undulators over a limited region of photon energy.

F. Data acquisition and analysis

In each of the two experiments, data were taken continuously in singles mode for both detectors and stored in list mode. No hardware coincidence logic was used. The data for each event consisted of a γ -ray energy, a label identifying the detector, and a 50-ns clock word that indicated the time with respect to the beginning of the irradiation cycle. The 50-ns clock word was synchronized with the removal of the W block that started the irradiation cycle.

Wilkinson-type analog-to-digital converters (ADCs) were used, which resulted in significant dead time. In addition, real-time histogramming contributed to dead time. These dead time losses were sampled every 1 ms and recorded in the list-mode data. Additional losses due to the analog electronics and pileup rejection circuitry in the amplifiers during the beam-on period were determined by comparing the measured area of the 1093.6-keV γ ray of ^{172}Lu in the beam-on spectra with the area from beam-off spectra, after correcting for ADC dead time. In the thin-target experiment, the pileup losses were 3–6% for the 20-mm-gap data and 10–15% for the 15-mm-gap data. Pileup losses for the thick-target experiment were up to $\sim 30\%$ for the highest-rate beam-target combinations listed in Table II.

The offline analysis was performed by sorting the list-mode data from each run into energy spectra, gated by the 50-ns clock word. Three equal-width time windows of 10.6 s were set on the time parameter in the data stream, corresponding to the beam-on (T_1) interval followed by two beam-off (T_2 and T_3) intervals. Data recorded during the short (~ 1.6 -s) interval between the irradiation and counting intervals were excluded in order to avoid effects of shutter movement, etc. A typical time spectrum, showing the three windows used in the sort, is presented in Fig. 10(a). The corresponding energy spectra are given in Figs. 10(b)–(d). The acquisition live time was determined for each time window by counting the number of “live” millisecond pulses for each ADC. The corresponding spectra

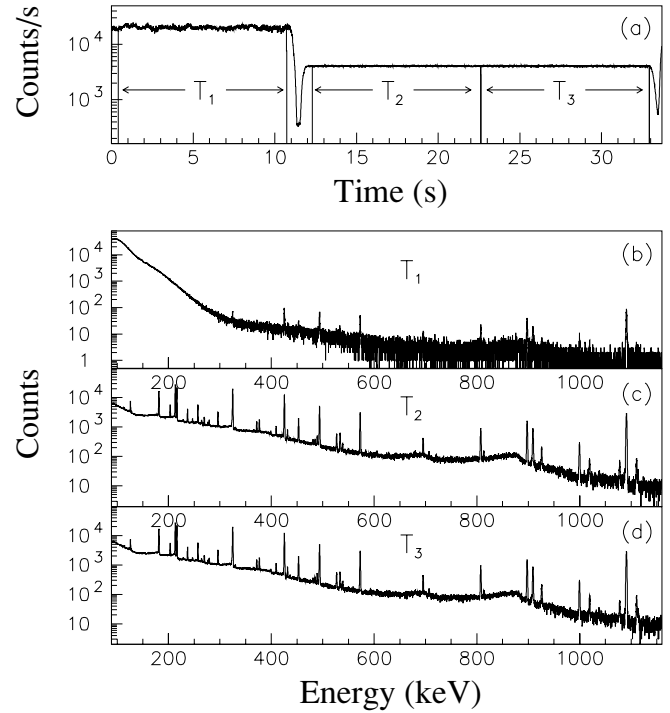


FIG. 10. Example of the accumulated spectra from the thick target R-1 for the time windows that were used in the offline sorting. The γ -ray spectra corresponding to the time gates (a) are presented in panels (b)–(d); see text for details. The data shown represent a total of about 4 h of accumulation. Note that panel (b) corresponds to the measurement while the photon flux was on and a Pb shutter was placed in front of the detector. Thus the total counting rate in this detector was high because of scattered leakage flux from the beam at low energies; but the counting rate from the hafnium source was attenuated at all energies (see also Fig. 13).

for the different time windows in the thin-target runs are shown in Fig. 11.

IV. RESULTS

A. Thick target

1. Out-of-beam, delayed limits

The 200–500-keV region of a typical beam-off spectrum, summed over the intervals T_2 and T_3 , taken with detector B is presented in Fig. 12. The spectrum was accumulated with target R-1 and undulator setting of 20 mm over a period of 8.5 h. Ground-state band γ rays emitted in the decay of $^{178}\text{Hf}^{m1}$ are highlighted. Similar results were found for all targets, all average undulator gap settings, and both detectors.

A beam-induced decay of the $K^\pi = 16^+$, $^{178}\text{Hf}^{m2}$ isomer would result in an increased production of the 4-s isomer, and the emission of the subsequent γ rays in the GSB during the beam-off period. In particular, this would result in an enhanced counting rate in interval T_2 as compared to T_3 (see Fig. 10).

The incremental nonequilibrium population Δ of the $K^\pi = 8^-$, $^{178}\text{Hf}^{m1}$ isomer after an irradiation time $T_1 = 10.6$ s is

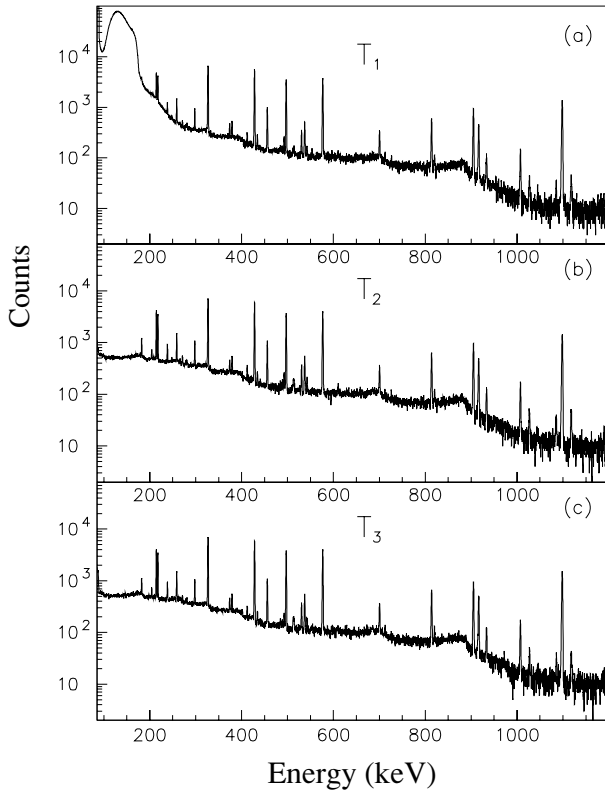


FIG. 11. The γ -ray spectra obtained in the thin-target experiment for the 20-mm-gap setting. The spectra correspond to the same time gates as described for the thick-target analysis. The data shown represent a total of about 30 h of accumulation time.

given by the equation

$$\begin{aligned} \Delta &= (N_{m2}/A)\phi\sigma_{\text{int}}\tau_{m1}(1 - e^{-T_1/\tau_{m1}}) \\ &= 0.84(N_{m2}/A)\phi\sigma_{\text{int}}\tau_{m1}, \end{aligned} \quad (4.1)$$

where N_{m2} is the number of $^{178}\text{Hf}^{m2}$ target atoms, A is the cross-sectional area of the beam at the target (4 mm² for the thick-target runs and 2.8 mm² for the thin target), ϕ is the incident number of photons per s keV, $\tau_{m1} = 5.8$ s is the mean life of $^{178}\text{Hf}^{m1}$, and σ_{int} is the integrated cross section for the postulated absorption in units of cm² s. The quantity σ_{int} includes contributions from any of the reported

narrow resonances or broader areas of enhancement within the integrating energy interval.

Data were not used for the time interval of 1.6 s while the W block moved into position to inhibit the beam and the detector shutters opened. During this time, Δ is reduced by a factor of $e^{-1.6/5.8} = 0.76$. As described above, the remaining beam-off period lasted 21.2 s, which was broken into two equal counting periods, T_2 and T_3 , of 10.6 s each. A nonequilibrium population will result in more $^{178}\text{Hf}^{m1}$ decays in period T_2 compared with T_3 by an amount

$$\begin{aligned} &0.64(N_{m2}/A)\phi\sigma_{\text{int}}\tau_{m1} \left(\int_0^{10.6} \frac{e^{-t/\tau_{m1}}}{\tau_{m1}} dt - \int_{10.6}^{21.2} \frac{e^{-t/\tau_{m1}}}{\tau_{m1}} dt \right) \\ &= 0.45(N_{m2}/A)\phi\sigma_{\text{int}}\tau_{m1} \\ &= \frac{C(T_2) - C(T_3)}{\beta\epsilon}, \end{aligned} \quad (4.2)$$

where β is the γ -ray intensity per disintegration [17], ϵ is the efficiency of the detector, and $C(T_2)$ and $C(T_3)$ are the livetime corrected counts observed in periods T_2 and T_3 , respectively, for detector channels corresponding to transitions in the ground-state band of ^{178}Hf . The difference in live times between periods T_2 and T_3 was always less than 0.5%.

When $\Delta \ll N_{m2}$, N_{m2} can be approximated as

$$N_{m2} \approx \frac{\tau_{m2}}{T_3} \frac{C(T_3) - B(T_3)}{\beta\epsilon}, \quad (4.3)$$

where $\tau_{m2} = 45$ yr is the mean life of $^{178}\text{Hf}^{m2}$ and $B(T_3)$ is the Compton-scattered photon background. This background was subtracted by using the flat upper limit (FUL) method developed by Crowell *et al.* [31] with a ruler length of 3.75 keV. A typical background spectrum determined with the FUL method is shown in Fig. 12. The FUL method has been shown to be both reliable and objective for this type of analysis [31]. The variance of the background was taken to be the number of background counts.

Equations (4.2) and (4.3) can be combined to give the relation

$$\sigma_{\text{int}} = \frac{AT_3}{0.45\phi\tau_{m1}\tau_{m2}} \frac{C(T_2) - C(T_3)}{C(T_3) - B(T_3)}, \quad (4.4)$$

which is independent of β , ϵ , and N_{m2} .

Results for γ -ray lines highlighted in Fig. 12 are summarized in Table VI for each target-gap combination. We found no statistically significant difference in the γ -ray intensities

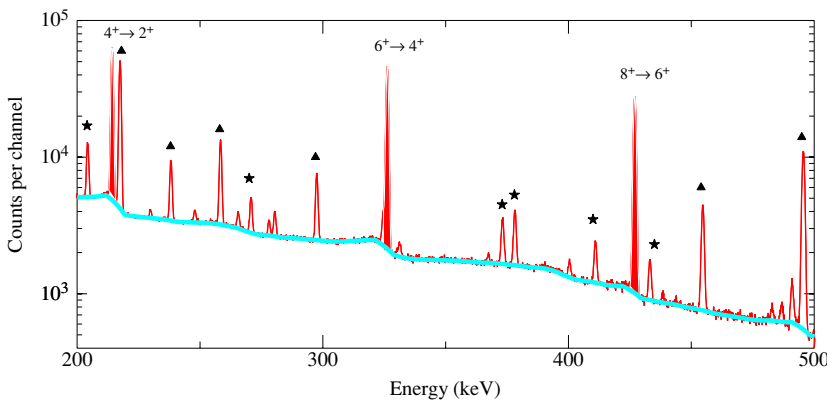


FIG. 12. (Color online) Typical thick-target beam-off γ -ray spectrum, summed over the intervals T_2 and T_3 . The photopeaks for the GSB transitions at 213, 326, and 426 keV are filled in. The transitions at 217, 237, 258, 297, 454, and 496 keV are from the band based on the 8^- isomer and are indicated with a triangle, with the other significant lines from the ^{172}Hf (^{172}Lu) contaminant marked by an asterisk. The dispersion is ~ 0.15 keV/channel. The Compton background determined from the FUL method [31] is shown as a thick gray curve.

TABLE VI. Out-of-beam thick-target percentage difference in counting rate, $[C(T_2) - C(T_3)]/C(T_3)$, in the GSB transitions.

Target	Average gap (mm)	426-keV $8^+ \rightarrow 6^+$	326-keV $6^+ \rightarrow 4^+$	213-keV $4^+ \rightarrow 2^+$	Combined
R-1	20.0	-0.19(.32)	-0.30(.28)	-0.15(.27)	-0.21(.17)
R-1	15.0	0.25(.23)	0.32(.20)	-0.08(.20)	0.16(.12)
R-2	20.0	-0.01(.18)	0.05(.16)	-0.23(.16)	-0.07(.10)
R-3	20.0	0.32(.25)	0.04(.23)	-0.06(.24)	0.09(.14)
R-3	15.0	-0.22(.28)	0.27(.26)	0.02(.28)	0.04(.16)
R-3	13.5	0.25(.25)	0.07(.21)	-0.07(.18)	0.05(.12)
All data		0.09(.10)	0.10(.09)	-0.12(.09)	0.01(.05)

between the periods T_2 and T_3 for any γ -ray line in the spectrum.

Using the combined result for all γ rays in Table VI, $[C(T_2) - C(T_3)]/[C(T_3) - B(T_3)] = (1 \pm 5) \times 10^{-4}$. Therefore, a 99% (3σ) confidence interval has an upper bound of 1.5×10^{-3} (Ref. [32]). In other words, there is a 99% chance that the true value of $[C(T_2) - C(T_3)]/[C(T_3) - B(T_3)]$ lies below 1.5×10^{-3} and a 1% chance that it lies above 1.5×10^{-3} . Similar results are obtained by comparing the total number of counts in the peak regions without background subtraction.

Using Eq. (4.4), a 99% upper limit of $\sigma_{\text{int}}(E) \leq 1.7 \times 10^{-13}/\phi(E)$ keV cm² is obtained, where E is the incident photon energy and $\phi(E)$ is in units of s⁻¹ keV⁻¹. These limits are statistically independent and combined with appropriate weights corresponding to each row of Table VI to obtain a limiting cross section for the data from the thick target, that sets the best limit for photon energies above ≈ 20 keV.

2. In-beam, prompt limits

For a postulated prompt deexcitation scenario, the process would occur only during the irradiation period and would bypass the $K = 8$, 4-s isomer. We searched for this mode by looking for an enhanced counting rate in the GSB transitions during irradiation compared with that with no beam. Here we used the 1093.6-keV transition from the decay of ¹⁷²Hf into ¹⁷²Lu to normalize the beam-on to the beam-off spectra, both taken with the Pb shutters in place. The uncertainty in this analysis is somewhat larger than in the beam-off analysis because the high background required peak fitting in order to extract the relevant yields during the beam-on period. Also, with the Pb shutter in place, the detection efficiency was lower. In Fig. 13, a typical beam-on spectrum is compared with a beam-off spectrum taken with the detector shutters closed.

In the beam-on/prompt analysis σ_{int} is given by the relation

$$\sigma_{\text{int}} = \frac{A}{\phi \tau_{m2}} \frac{C(T_1) - C_b}{C_b}, \quad (4.5)$$

where C_b is the number of counts in the photopeaks in the normalized background spectrum. Since the induced decay in this scenario bypasses ¹⁷⁸Hf^{m1}, a positive result will enhance the counting rate of the GSB transitions relative to beam off. Because the shutters moved in and out during the irradiation cycling, the background rate C_b that is relevant to the in-beam measurements had to be determined with the

shutter in place, in a separate continuous measurement with no beam.

Results are summarized in Table VII for each target-gap combination. The quoted uncertainties include estimates of the systematic uncertainties for the peak and background shapes. No significant increase in counting rate for any transition in the GSB was observed. A 99% confidence interval for $[C(T_1) - C_b]/C_b$ has an upper bound of 2.8×10^{-2} . For comparison, the same analysis was performed for transitions in the $K = 8$ band. These results, summarized in Table VIII, are consistent with those for the GSB. Using the combined result for all γ rays in Table VII and Eq. (4.5), a 99% confidence upper limit

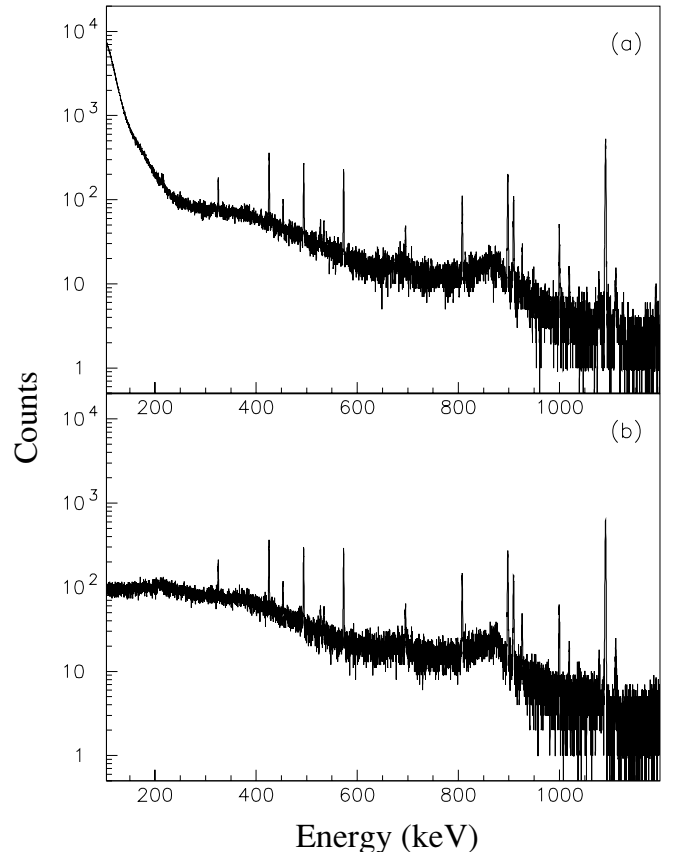


FIG. 13. Typical thick-target spectra for (a) beam on and (b) beam off. Both spectra were measured with the detector shutters in the closed position. Note the additional low-energy background in (a) induced by the scattered beam.

TABLE VII. Beam-on vs. beam-off thick-target percentage difference in counting rate, $[C(T_1) - C_b]/C_b$, for promptly induced transitions in the GSB.

Target	Average gap (mm)	426-keV $8^+ \rightarrow 6^+$	326-keV $6^+ \rightarrow 4^+$	213-keV $4^+ \rightarrow 2^+$	Combined
R-1	20.0	9.6(12.6)	3.6(22.7)	—	8.2(11.0)
R-2	20.0	-0.1(1.9)	-1.2(4.0)	2.0(5.9)	-0.1(1.6)
R-3	20.0	0.3(2.5)	-0.4(3.8)	0.4(5.1)	0.1(1.9)
R-3	15.0	2.6(4.3)	-12.2(9.1)	—	-0.1(3.9)
R-3	13.5	0.8(2.0)	-0.7(4.0)	-12.9(18.9)	0.4(1.8)
All data		0.6(1.2)	-1.4(2.2)	0.5(3.8)	0.2(1.0)

TABLE VIII. Beam-on vs. beam-off thick-target percentage difference in counting rate, $[C(T_1) - C_b]/C_b$, for promptly induced transitions in the $K^\pi = 8^-$ band.

Target	Average gap (mm)	574-keV $13^- \rightarrow 11^-$	495-keV $11^- \rightarrow 9^-$	454-keV $10^- \rightarrow 8^-$	Combined
R-1	20.0	9.6(14.4)	-4.0(13.5)	43.7(65.4)	3.3(9.7)
R-2	20.0	-1.4(2.4)	-1.0(2.6)	1.4(6.6)	-1.0(1.7)
R-3	20.0	1.3(2.1)	-0.1(2.1)	-1.0(7.4)	0.5(1.5)
R-3	15.0	2.4(4.5)	1.6(5.1)	8.2(19.9)	2.2(3.3)
R-3	13.5	0.2(1.8)	-0.4(2.7)	2.1(8.0)	0.1(1.5)
All data		0.4(1.1)	-0.3(1.3)	1.3(4.1)	0.1(0.9)

of $\sigma_{\text{int}}(E) \leq 7.9 \times 10^{-13}/\phi(E)$ keV cm² in this decay scenario is obtained.

B. Thin target

1. Out-of-beam, delayed limits

The out-of-beam analysis for the thin-target data was performed in exactly the same manner as for the thick-target data. The 200–500 keV region of the beam-off spectrum from the data taken with the 20-mm-gap setting is shown in Fig. 14. The results for the beam-off analysis are summarized in Table IX. Using these results and Eq. (4.4), a 99% upper limit of $\sigma_{\text{int}}(E) \leq 1.5 \times 10^{-12}/\phi(E)$ keV cm² is obtained.

2. In-beam, prompt limits

In the thin-target measurement, no movable shutters were used during the beam-on period. It was, therefore, possible to make a direct comparison of the γ -ray intensities during irradiation with those from the corresponding beam-off interval. In this case, the second beam-off counting period was used as the “background” spectrum. The comparison is complicated because the scattered x-ray beam entering the detector increased the background and dead time in the measured beam-on γ -ray spectrum (see Fig. 11). Peak fitting was used to extract the γ -ray intensities from the beam-on spectra for comparison with the beam-off values. To correct for differences due to pileup effects and dead time losses in the electronics, the spectra were normalized using the 1093.6-keV line in ¹⁷²Lu.

The results are summarized in Table X for the data sets with the two gap settings and the two values of absorber for the 15-mm settings listed in Table III. The quoted uncertainties include systematic uncertainties for the peak and background shapes. No significant increase in counting rate for any transition in the GSB was observed. A 99% confidence interval for $[C(T_1) - C(T_3)]/C(T_3)$ has an upper bound of 5.2×10^{-2} . For comparison, the same analysis was performed for transitions in the $K = 8$ band. These results are summarized in Table XI and are consistent with the ground-state band. Using the combined result for all γ rays in Table X and Eq. (4.5), a 3σ (99% confidence) upper limit of

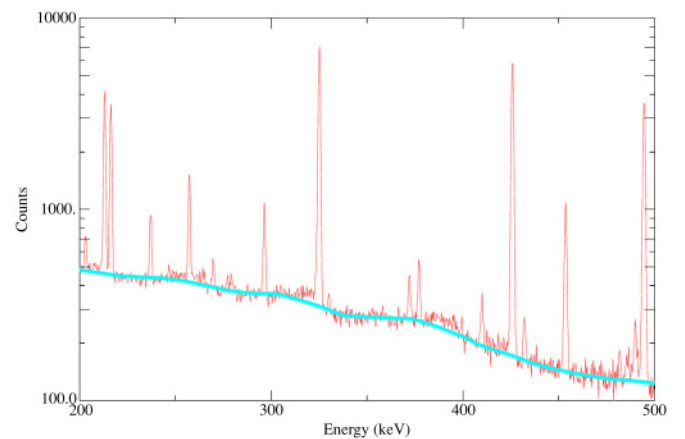


FIG. 14. (Color online) Beam-off γ -ray spectrum from the thin-target, 20 mm gap data set, with a dispersion of ~ 0.15 keV/channel. The Compton background determined from the FUL method [31] is the smooth thick grey curve.

TABLE IX. Out-of-beam thin-target percentage difference in counting rate, $[C(T_2) - C(T_3)]/C(T_3)$, for transitions in the GSB.

Average gap (mm)	426-keV $8^+ \rightarrow 6^+$	326-keV $6^+ \rightarrow 4^+$	213-keV $4^+ \rightarrow 2^+$	Combined
20.0	0.47(.96)	-0.15(.94)	0.74(1.44)	0.26(.61)
15.0(a)	-3.6(2.6)	-2.6(3.5)	—	-3.2(2.1)
15.0(b)	3.1(2.4)	-5.6(2.4)	—	-1.2(1.7)
All data	0.40(.84)	-0.98(.85)	0.74(1.44)	-0.14(.55)

TABLE X. Beam-on vs. beam-off thin-target percentage difference in counting rate, $[C(T_1) - C(T_3)]/C(T_3)$, for promptly induced transitions in the ground-state band.

Average gap (mm)	426-keV $8^+ \rightarrow 6^+$	326-keV $6^+ \rightarrow 4^+$	213-keV $4^+ \rightarrow 2^+$	Combined
20.0	1.4(3.4)	0.4(3.2)	-0.3(4.0)	0.5(2.0)
15.0(a)	-2.4(8.3)	-0.1(9.4)	-2.2(11.1)	-1.6(5.4)
15.0(b)	7.2(8.4)	4.2(8.3)	-6.4(9.4)	2.3(5.0)
All data	1.6(2.9)	0.8(2.8)	-1.3(3.5)	0.5(1.8)

TABLE XI. Beam-on vs. beam-off thin-target percentage difference in counting rate, $[C(T_1) - C(T_3)]/C(T_3)$, for promptly induced transitions in the $K^\pi = 8^-$ band.

Average gap (mm)	574-keV $13^- \rightarrow 11^-$	495-keV $11^- \rightarrow 9^-$	454-keV $10^- \rightarrow 8^-$	Combined
20.0	2.0(3.2)	1.2(3.3)	4.2(4.5)	2.2(1.8)
15.0(a)	1.3(8.7)	-4.5(9.8)	—	-1.3(6.5)
15.0(b)	-0.3(8.0)	2.2(10.3)	—	0.6(6.3)
All data	1.6(2.8)	0.8(3.0)	4.2(4.5)	1.9(1.7)

$\sigma_{\text{int}}(E) \leq 1.0 \times 10^{-12}/\phi(E)$ keV cm² in this decay scenario is obtained, very similar to the limit obtained for the delayed emission.

In addition to the limits on the known transitions discussed above, our data allow us to address the question of the 129-keV transition reported by Collins *et al.* [15], a transition that has not been otherwise seen in ¹⁷⁸Hf. This transition was reported to be observed only during irradiation of the ¹⁷⁸Hf^{m2} sample. Based on γ - γ coincidence data, it was proposed [15] that following excitation, this γ ray is part of a cascade that also includes the 213-keV GSB transition, bypassing the higher-lying members of the GSB, and the $K^\pi = 8^-$ band.

If this scenario were indeed the case, then we would not expect to see any enhancement of the GSB transitions in the first beam-off interval compared to the second. However, we should definitely observe an enhancement of the 213-keV GSB transition during irradiation. We saw no such enhancement, as indicated in Table VII, column 4.

With this scenario, we would also expect to see evidence for the 129-keV line. In our experimental arrangement, it was necessary to use an absorber package to maintain a reasonable counting rate of x rays produced by the scattered beam. This package also reduced the transmission of \sim 129-keV γ rays from the Hf target, as shown in Fig. 5. Therefore,

the sensitivity of our measurement to the 129-keV line was substantially lower than that for the 213-keV transition. To place a limit on the excitation of the proposed [15] 129-keV transition, we used the MCNP simulation mentioned above with the detector/absorber configuration used in the 20-mm-gap measurement.

In the simulation, 10^9 129-keV photons were propagated through the absorbers and into the detector, and a “pulse-height (F8) tally” (see Ref. [23]) for the Ge crystal was recorded. This same approach was used in the simulation of the efficiency for higher-energy γ rays that were shown in Fig. 5, where the agreement between the calculated and the measured efficiencies was generally better than 10%. Illustrating the expected yield in the 129-keV line for the scenario proposed in Ref. [15], Fig. 15 shows a simulated spectrum added onto the observed one for an emission rate calculated for the cross section reported: 2.2×10^{-22} cm² keV under the conditions of our measurement. The lower part of Fig. 15 shows a similar spectrum under the assumption that the 129-keV γ ray is in coincidence with the 213-keV GSB transition 100% of the time for the same value of the cross section. There is no evidence for a 129-keV line, with a limiting integral cross section of $\approx 5 \times 10^{-24}$ cm² keV, if the 129-keV transition bypasses the ground-state band completely. Moreover, there is no evidence for an increase in the known 213-keV line, reported to be in

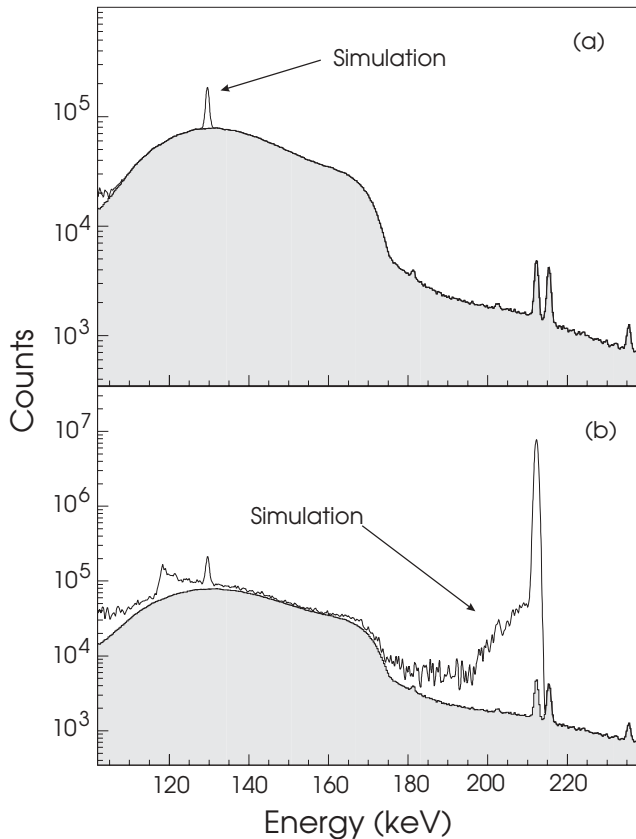


FIG. 15. Simulated γ -ray spectra superimposed on the measured in-beam spectrum (shaded) obtained for the 20-mm-gap setting. (a) The intensity of the 129-keV γ ray that would be expected if the cross section for the stimulated decay of the isomer were the reported value [15] of $2.2 \times 10^{-22} \text{ cm}^2 \text{ keV}$, and bypassed the GSB. (b) The simulated spectrum corresponding to the same cross section if the 129-keV γ ray were in coincidence with the 213-keV ground-state transition 100% of the time and bypassed the rest of the GSB.

coincidence with the 129-keV transition, with a limit below $\approx 10^{-26} \text{ cm}^2 \text{ keV}$.

V. DISCUSSION AND SUMMARY

The various limits obtained in percentage change in counting rates are summarized in Table XII. The limits on integral cross sections were derived with the known fluxes, corrected for absorption within the target, and allowing for the systematic errors discussed earlier. The excluded regions corresponding to these limits, derived using Eqs. (4.4) and (4.5), are shown

TABLE XII. Summary of 99% confidence limits, including systematic errors, on a possible difference in counting rates obtained from the present measurements and, in parentheses, $\sigma_{\text{int}}/\phi(E) \text{ keV cm}^2$.

Target	Out-of-beam—delayed	In-beam—prompt
Thick	0.15% (1.5×10^{-13})	2.8% (7.9×10^{-13})
Thin	1.9% (1.3×10^{-12})	5.2% (1.0×10^{-12})

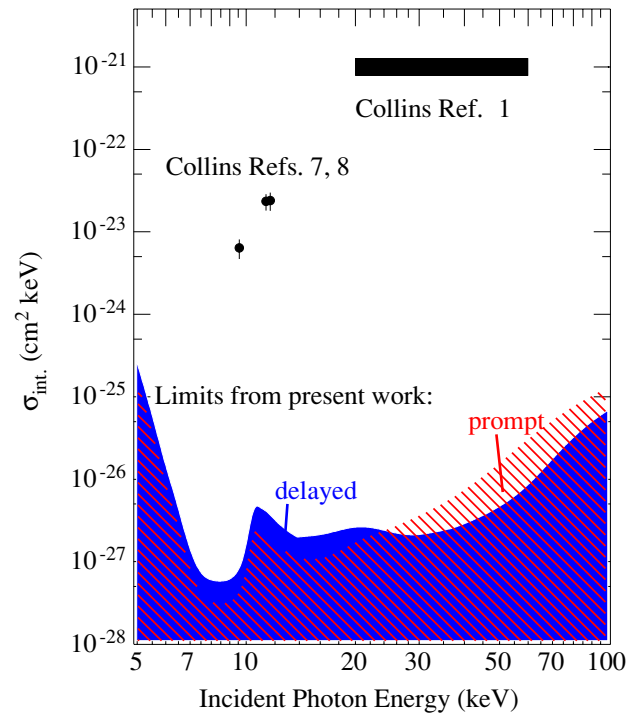


FIG. 16. (Color online) Limiting cross sections (99% confidence limit, including systematic errors) for the cross sections corresponding to all the data in the present measurement for the photon-induced deexcitation of the $K\pi = 16^+ \text{ }^{178}\text{Hf}^{m2}$ isomer. The limits show the combined result for the thick and thin targets. The areas above the gray and hatched regions are excluded by the present measurements, with the (red) hatched area corresponding to the limit for prompt, in-beam deexcitation, and the gray (blue) region showing the slightly different limit at high x-ray energies for a delayed one. The values corresponding to the positive results from the measurements of [30] and [7] are also shown.

in Fig. 16 where the area above the shaded region is excluded. The slight differences between the excluded regions for prompt and delayed triggering are shown in different shades. The thick- and thin-target limits are combined in the figure; the two give comparable values between 10 and 20 keV; at lower energies, the limit is set by the thin-target measurement while above 20 keV, thick-target limits are lower by a factor that is increasing to ≈ 4 . Because of the more detailed statistical analysis used, the present limits, while similar in magnitude, are slightly different from the ones in our previous publications [10,11].

The intent of this work was to see whether the effect reported by Collins *et al.* could be reproduced. We observed no signs of enhancement with x-ray intensities covering the same region of energies at much higher intensities than those from the dental x-ray machine of [30]. The more recent work of the Collins collaboration [7], with x rays selected by a monochromator (nominal width of 1 or 0.1 eV) at a light source, reported effects over limited regions of x-ray energy, one apparently extending over about 70 eV, the other two over about 100 eV. If such triggering is real, then a continuous x-ray spectrum that overlaps *all* of these regions must also produce the triggering at *all* the appropriate energies simultaneously. The beam

TABLE XIII. Summary of results on triggering cross sections $^{178}\text{Hf}^{m2}$.

Source	Energy (keV)	Integrated cross section (barn keV)
Dental x ray [1,5]	20–40	200–1000
SPring-8 [7]	11.3, 11.7, 9.56	23, 24, 6
NSLS [33]	Selected regions between 9.3 and 13.5 keV	<0.1
Present work	8–30	<0.003 (prompt)
(99% confidence limit)		<0.005 (delayed)

intensities per unit energy interval from the two light sources are similar and the only significant difference is that in the present measurements the regions of reported enhancement are covered at the same time. Thus, if there is enhancement in the decay of the isomer with the monochromatic x rays at certain energies, then there has to be a much larger (at least 100-fold) enhancement with the white beam. In other words, each (0.1–1 eV) step at which enhancement was reported in [7] would have to be contributing simultaneously and cumulatively in our measurement. The specific photon fluxes are comparable, but our experiment irradiates the sample for a much longer time than the time taken for each step with the monochromator. All these factors are taken into account quantitatively in the cross-section limits.

Our combined results on limits to the integral cross section for any deexcitation processes for the hafnium isomer may be compared to what would be expected, based on the values of Refs. [1,5,6,8,30], where it was found that the decay transitions were enhanced (accelerated) by 2–6%. The comparison is shown in Table XIII and includes a recent negative result with a monochromatized x-ray beam at the BNL National Synchrotron Light Source (NSLS) [33].

Our negative result here in no way contradicts the positive results found for the induced decay of an isomer in ^{180}Ta (at an excitation energy of 75 keV and with a half-life greater than 10^{15} yr) when bombarded with high-energy bremsstrahlung [14]. They report integral cross sections for depopulating the isomer with bremsstrahlung with endpoints between 1 and 2.8 MeV with photons that are about two orders of magnitude higher in energy than in the experiments of Collins *et al.* The reported values for the cross sections range between 5×10^{-29} and 4×10^{-26} keV cm², which are much lower than the

10^{-22} keV cm² range reported by Collins *et al.* For these high-energy photons, the cross sections are of the expected order of magnitude, since dipole radiation widths increase as the photon energy cubed.

Using the level of stimulated emission observed for the isomer in ^{180}Ta to extrapolate from the 1000-keV photon energy in that measurement to the 10-keV region that is relevant here would give an expected cross section in the range of 10^{-6} barn keV, or 10^{-30} keV cm². This is certainly consistent with our negative result.

We have carried out a high-sensitivity, broadband search for x-ray-induced decay of $^{178}\text{Hf}^{m2}$ using a variety of targets in an intense x-ray beam. We see no evidence for an x-ray induced decay of the 31-yr isomer of ^{178}Hf , either delayed, through the 4-s isomer, or prompt during the irradiation.

ACKNOWLEDGMENTS

We are indebted to J. Greene, R. V. F. Janssens, T. L. Khoo, C. J. Lister, R. Nelson, W. Patterson, K. Teh, and P. Garrett for their help in various aspects of these measurements, and to D. R. Haeffner, D. M. Mills, and G. Shenoy for their encouragement of this investigation at the XOR 1-ID beamline. This work was supported in part by the Office of Nuclear Physics and the Office of Basic Energy Sciences, U.S. Department of Energy (DOE) under Contract No. W-31-109-ENG-38 (ANL), in part by the DOE under Contract Nos. W-7405-ENG-48 (UC-LLNL), and W-7405-ENG-36 (UC-LANL), and in part by the DOE Nuclear Energy Research Initiative.

- [1] C. B. Collins, *et al.*, Phys. Rev. Lett. **82**, 695 (1999).
 [2] *New Scientist*, February 22, 2003, p. 4; *New Scientist*, July 3, 1999, p. 42; Science **283**, 769 (1999); C. R. Hartsfield, M.S. thesis, Air Force Institute of Technology, 2001, AFIT/GAE/ENY/01M-04; C. E. Hamilton, M.S. thesis, Air Force Institute of Technology, 2001, AFIT/GAE/ENY/02–6.
 [3] *New Scientist*, August 16, 2003, p. 4; *Popular Mechanics*, May 2004, p. 98.
 [4] S. Olariu and A. Olariu, Phys. Rev. Lett. **84**, 2541 (2000); D. P. McNabb *et al.*, *ibid.* **84**, 2542 (2000); P. von Neumann-Cosel and A. Richter, *ibid.* **84**, 2543 (2000).
 [5] C. B. Collins *et al.*, Phys. Rev. C **61**, 054305 (2000).
 [6] C. B. Collins *et al.*, Phys. At. Nucl. **63**, 2067 (2000).

- [7] C. B. Collins *et al.*, Europhys. Lett. **57** (5), 677 (2002).
 [8] C. B. Collins *et al.*, Laser Phys. **14**, 1 (2004).
 [9] E. V. Tkalya, Phys. Rev. C **68**, 064611 (2003).
 [10] I. Ahmad *et al.*, Phys. Rev. Lett. **87**, 072503 (2001).
 [11] I. Ahmad *et al.*, Phys. Rev. C **67**, 041305(R) (2003).
 [12] D. S. Gemmell, in *Proceedings of the 19th International Conference on X-ray and Inner-Shell Processes, Rome, 24–28 June 2002* (American Institute of Physics, Melville, NY, 2003), Vol. 652, p. 239.
 [13] J. A. Becker, D. S. Gemmell, J. P. Schiffer, and J. B. Wilhelmy, Europhys. Lett. **61**, 721 (2003).
 [14] D. Belic *et al.*, Phys. Rev. C **65**, 035801 (2002); P. M. Walker, G. D. Dracoulis, and J. J. Carroll, *ibid.* **64**, 061302 (2001).

- [15] C. B. Collins *et al.*, *Hyperfine Int.* **135**, 51 (2001).
- [16] J. van Klinken *et al.*, *Nucl. Phys.* **A339**, 189 (1980); P. M. Walker and G. D. Dracoulis, *Nature* **399**, 35 (1999); M. B. Smith *et al.*, *Phys. Rev. C* **68**, 031302R (2003).
- [17] E. Browne, *Nucl. Data Sheets* **72**, 221 (1994).
- [18] S. Deylitz *et al.*, *Phys. Rev. C* **53**, 1266 (1996).
- [19] E. Lubkiewicz *et al.*, *Z. Phys. A* **355**, 377 (1996).
- [20] S. M. Mullins, G. D. Dracoulis, A. P. Byrne, T. R. McGoram, S. Bayer, W. A. Seale, and F. G. Kondev, *Phys. Lett.* **B393**, 279 (1997).
- [21] A. B. Hayes *et al.*, *Phys. Rev. Lett.* **89**, 242501 (2002).
- [22] B. Lai *et al.*, Argonne National Laboratory Report ANL/APS/TB-3, 1993 (unpublished); R. J. Dejus *et al.*, Argonne National Laboratory Report ANL/APS/TB-17, 1994 (unpublished).
- [23] X-5 Monte Carlo Team, Los Alamos National Laboratory Report LA-CP-03-0245, 2003 (unpublished).
- [24] M. B. Smith *et al.* *Phys. Rev. C* **68**, 031302(R) (2003).
- [25] M. J. Berger, J. H. Hubbell, S. M. Seltzer, J. S. Coursey, and D. S. Zucker, *NIST Standard Reference Data Base (XGAM)*, <http://physics.nist.gov/PhysRefData/Xcom/Text/XCOM.html>.
- [26] B. Singh, *Nucl. Data Sheets* **75**, 199 (1995).
- [27] S. D. Shastri, R. J. Dejus, and D. R. Haeffner, *J. Synchrotron Rad.* **5**, 67 (1998).
- [28] R. J. Dejus and A. Luccio, *Nucl. Instrum. Methods A* **347**, 61 (1994).
- [29] C. T. Chantler, *J. Phys. Chem. Ref. Data* **24**, 71 (1995).
- [30] C. B. Collins *et al.*, *Laser Phys.* **9**, 8 (1999).
- [31] B. Crowell, M. P. Carpenter, R. G. Henry, R. V. F. Janssens, T. L. Khoo, T. Lauritsen, and D. Nisius, *Nucl. Instrum. Methods Phys., Ser. A* **355**, 575 (1995).
- [32] G. J. Feldman and R. D. Cousins, *Phys. Rev. D* **57**, 3873 (1998).
- [33] H. E. Roberts *et al.*, *Hyperfine Int.* **143**, 111 (2002); J. J. Carroll, *Laser Phys. Lett.* **1**, 275, 2004.